

Received 3 September 2023, accepted 9 September 2023, date of publication 12 September 2023, date of current version 22 September 2023.

Digital Object Identifier 10.1109/ACCESS.2023.3314510

RESEARCH ARTICLE

Research on Bidirectional On-Board Charging System Based on Three-Phase Wye-Wye Connected CLLC Resonant Converter

KAI ZHOU¹, YIWEN HUANG¹, AND SHAOLONG ZHENG¹

Engineering Research Center of Automotive Electronics Drive Control and System Integration (Ministry of Education), Harbin University of Science and Technology, Harbin 150080, China

Corresponding author: Yiwen Huang (H775843019@163.com)

This work was supported by the Heilongjiang Provincial Natural Science Foundation of China under Grant LH2021E086.

ABSTRACT The traditional on-board charging system can only realize the one-way transmission of electric energy from the grid to the power battery. To address this issue, this paper proposes a bidirectional on-board charging system based on a three-phase wye-wye connected CLLC resonant converter. It adopts a two-stage structure, the front-stage is a bidirectional totem pole converter and the rear-stage is a three-phase wye-wye connected CLLC resonant converter. Based on the grid characteristics, the working principle of the front-stage converter is analyzed, the equivalent circuit model of the rear-stage converter is derived using fundamental wave analysis, and the voltage gain, impedance characteristics and zero voltage turn-on conditions are analyzed. The parameters of input inductor, DC bus capacitance and resonant network are calculated according to the design specifications of the bidirectional on-board charging system. The control strategy of bidirectional vehicle charging system is studied. The input current and input voltage are kept in the same phase by establishing the small signal circuit model of the front-stage bidirectional totem pole converter. The rear-stage three-phase wye-wye connected CLLC resonant converter adopts pulse frequency modulation to realize constant voltage and constant current output of the charging system. Simulation software was used to simulate the bidirectional on-board charging system, and a 3.3 kW prototype was trial-produced according to the main circuit parameters. Simulation and experimental results verify the correctness of the design of the bidirectional on-board charging system.

INDEX TERMS Bidirectional on-board charging system, resonant converter, three-phase wye-wye connected, totem pole converter.

I. INTRODUCTION

In the field of conductive on-board charging, two-stage on-board charging systems are widely used due to their many advantages. An on-board charging system is a special device that is fixed on the electric vehicle, converts AC power into DC power, and charges the power battery by means of conduction [1]. Conventional on-board charging systems can only achieve a one-way flow of energy from the grid to the electric vehicle, in order to meet the development demand of intelligence, the on-board charging system starts to develop in the direction of supporting the bidirectional flow of energy,

The associate editor coordinating the review of this manuscript and approving it for publication was Zhilei Yao¹.

so as to realize the bidirectional conversion of energy between grid voltage and battery voltage [2]. Moreover, the possibility for electric vehicles to deliver power back to the grid has increased the interest in bidirectional power flow solutions in the automotive market [3]. Reference [4] introduces the structure of a possible charging station (CS), which integrates three power supply modes: ac utility grid, PV modules and a diesel generator.

The bidirectional on-board charging system proposed in this paper is shown in Fig. 1. Its charging function is generally consistent with reference [4], that is, the power grid supplies power to the vehicle power battery. For the inverter function, the system proposed in reference [4] allows the integration of the utility grid and renewable energy sources, e.g., PV and

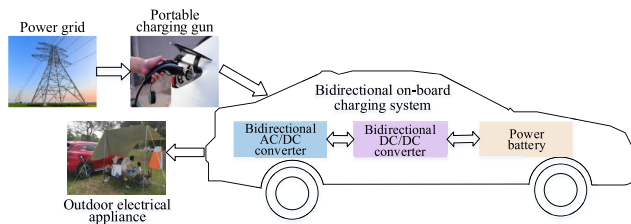


FIGURE 1. Bidirectional on-board charger system structure and application.

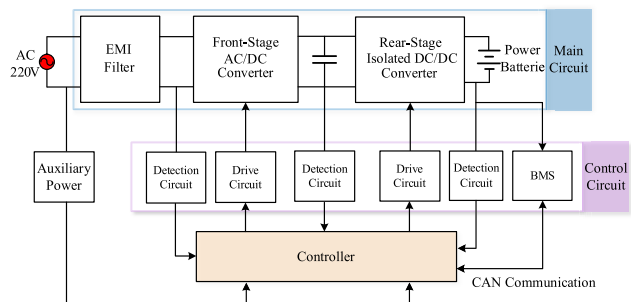


FIGURE 2. Structure of on-board charging system.

wind, where the energy surplus can be injected into the ac grid. The system proposed in this paper does not have the grid-connected function, and the inverter function proposed means that the battery supplies power to external loads such as outdoor electrical appliances under outdoor conditions.

The on-board charging system mostly adopts a two-stage structure, which is shown in Fig. 2.

The front-stage circuit is an AC/DC converter, which is mainly used to achieve power factor correction to reduce the harmonic pollution of the charging system to the grid and to supply power to the rear-stage and auxiliary power supply; the rear-stage is a DC/DC converter, which directly provides electrical isolation and corresponding charging conditions for the electric vehicle power battery.

The front-stage AC/DC converter usually adopts the non-isolated structure, which can be divided into: matrix converter, multi-level converter and bridge converter according to the topology. Matrix type bidirectional AC/DC converter can achieve electrical isolation between input and output by introducing high frequency transformer, and has strong anti-interference ability and wide range of rising and falling voltage, however, matrix converters use more switching transistors and have complex energy transfer paths, which are easily restricted by the application [5]. Reference [6] shows a three-phase voltage-source converter based isolated matrix-type AC/DC converter. The high-frequency transformer takes the role of the line-frequency transformer, and the intermediate electrolytic capacitors used in a traditional two-stage power conversion system are no longer required. With the increase of voltage level and power level, some diode, fly-across capacitor clamps and cascaded multilevel converters

have been widely studied [7]. Compared with two-level converters, the three-level converters have the advantages of low switching transistor voltage stress, smooth waveform, small filter inductance, and wide gain range [8]. A three-level converter is proposed in the reference [9], but due to its problem of unbalanced capacitor midpoint potential, complex control strategies need to be used to achieve the midpoint potential balance, while the complexity and failure rate of the control system are affected as the number of switching transistors increases. A bridge converter is proposed in [10], which has significant advantages in terms of size, cost, and reliability, and has good soft-switching as well as power regulation capability, the modeling determines the optimal modulation strategy, which greatly reduces the total circuit losses. In addition, the full-bridge AC/DC converter has less voltage stress and can be applied to larger power applications.

The rear-stage DC/DC converter mostly adopts isolation type structure. Bidirectional DC/DC converters have been widely used in battery charging and discharging management equipment such as battery formation, energy storage systems, and electric on-board charging piles [11]. The challenge and focus of DC/DC converter design has always been how to attain high power density and high efficiency. The volume of the transformer, inductor, and filter circuit can be significantly reduced by increasing the switching frequency, which is a practical technique to achieve high power density [12]. At present, LLC resonant converter is widely used in on-board charging system because of its simple structure, high power density, soft switching, wide voltage gain and other advantages [13]. The conventional LLC resonant converter uses fully controlled devices on the secondary-side instead of diodes in order to realize bidirectional flow of energy. The output voltage is regulated by controlling the operating frequency of the primary-side switching transistor during forward operation, and rectification is realized by the secondary-side switching transistor; in reverse operation, the reverse boost cannot be achieved because the excitation inductance is clamped by the output-side voltage. Reference [14] proposed modified three-phase LLC resonant converter. Compared to a conventional three-phase LLC converter, the modified topology has two more small, low power rated diodes. The proposed modified converter provides two-phase and single-phase operations of the circuit. These provide light-load efficiency improvement, and extended gain range for covering the dead zone charging of a battery, receptively. The proposed technique delivers the whole package of features needed by a three-phase LLC resonant converter in a high-power battery charger application. Reference [15] shows an asymmetric bidirectional CLLC resonant converter, which achieves bidirectional boosting by adding resonant capacitors on the secondary-side, which leads to inconsistent operating characteristics in forward and reverse operation due to the asymmetric structure of its transformer primary and secondary sides, which increases the difficulty of parameter design. In order to maintain structural symmetry,

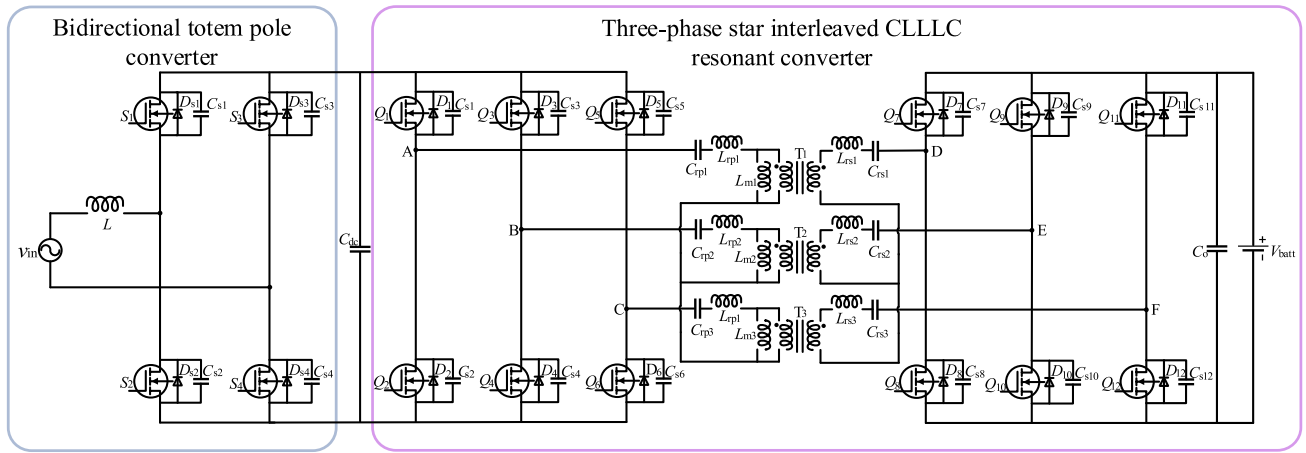


FIGURE 3. Topology of bidirectional on-board charging system.

reference [16] shows a CLLC resonant converter that introduces a set of resonant networks on the secondary-side of the LLC resonant converter, so the equivalent circuits are the same in forward and reverse operation. Reference [17] shows the gain characteristics, impedance characteristics, errors and floating of resonance parameters of the CLLC resonant converter in detail, under suitable operating conditions, the CLLC resonant converter has the good characteristics of the LLC resonant converter when the circuit parameters are symmetrical, and it is a bidirectional DC/DC converter that is more studied and more recognized by scholars at home and abroad. Reference [18] shows a family of two-phase interleaved LLC resonant converter with hybrid rectifier. By adaptively altering the hybrid rectifier configuration, the output voltage range is increased while the LLC resonant tank's conduction losses, circulating current, and switching frequency range are all decreased. With the increase of charging power, large capacity filter capacitors occupy a lot of space, for this problem, scholars at home and abroad proposed the interleaved parallel connection technology, interleaved parallel connection can effectively reduce the output current ripple, and reduce the number of filter capacitors used [19], [20], [21]. At present, the interleaved parallel technology is divided into two-phase interleaved parallel and three-phase interleaved parallel [22]. Two-phase interleaved parallel CLLC resonant converter, the amplitude of output current ripple is about one-tenth of single-phase CLLC resonant converter, however, the problem of uneven current between two converters may exist in the operation of the two-phase interleaved parallel CLLC resonant converter [23]. For three-phase direct interleaved parallel CLLC resonant converter, because the parallel connection form is the same as two-phase interleaved parallel connection form, so there is also the problem of uneven flow, moreover, the three-phase direct interleaved parallel CLLC resonant converter has more switching transistors, larger losses, and complex control [24].

The technical specifications and comparison of the converters in the references are shown in Table 1. To solve the above problems, this paper proposes a bidirectional on-board charging system based on three-phase wye-wye connected CLLC resonant converter, which adopts two-stage isolation structure.

The advantages of the front-stage AC/DC converter structure are as follows:

- 1) Using single-phase bridge structure, although the number of switching transistors is twice as much as the bidirectional half-bridge AC/DC converter, the voltage stress is greatly reduced, so it can be applied to higher power occasions.
- 2) The two diodes in the traditional totem pole circuit are replaced by controllable switching devices to realize the bidirectional flow of energy.
- 3) The structure is relatively simple, which greatly reduces the complexity of control.

The advantages of the rear-stage DC/DC converter structure are as follows:

- 1) The bidirectional flow of energy can be realized, and the rear-stage CLLC resonant converter maintains symmetry in structure, that is, the equivalent circuit of the CLLC resonant converter can maintain consistency in structure regardless of the positive and negative working states, which greatly reduces the difficulty of parameter design.
- 2) The use of three-phase interleaved parallel can effectively reduce the output current ripple, and reduce the number of filter capacitors, so that the phase current is reduced. Compared with the three-phase direct parallel resonant converter, it greatly reduces the number of switching transistors and the complexity of the control system.
- 3) The primary and secondary sides of the transformer adopt three-phase bridge structure, and the primary and secondary sides are wye-wye connected, and the neutral point is not grounded, so it is easier to realize the interleaved parallel current sharing of the three-phase resonant converter.

TABLE 1. Technical specifications and comparison of converters in reference.

Topology	Ref	Structure	Power (kw)	Freq. (kHz)	Out. Volt. (V)	No. of Sw. /Diodes	Peak Efficiency (%)	Major Advantages/Disadvantages	
Bidirectional AC/DC Converter	[4]	Three-level Stacked Neutral-point-clamped Converter	2	25	230	18/24	95.8%	High power factor, low filtering requirement and low harmonic content.	The number of switching transistors is large, which increases the volume cost.
	[5]	Matrix Converter +Full Bridge Converter	-	75	48	16/16	-	High efficiency, high power density, low current harmonics, low unit power factor.	The number of switching transistors is large, the energy transmission is complex, and the application field is easy to be limited.
	[6]	Isolated Matrix-type AC/DC Converter	1	20	130	15/15	95.9	The electrolytic capacitors were saved with the single-stage power conversion, which can prolong the system life and reduce the failure rate	The control is complicated, the number of switching transistors is large, and the efficiency is low.
	[9]	NPC Type Three Level Converter	-	9	350	12/18	-	The switching transistor has the advantages of small voltage stress, smooth waveform, small filter inductance, wide gain range, and is suitable for high-power occasions.	The capacitor midpoint potential is not balanced, the number of switching transistors is large, which increases the volume cost, and the complexity and failure rate of the control system are greatly increased.
	[10]	Dual Active Bridge Converter	1	50	-	8/8	98.9%	The bidirectional flow of energy can be achieved, which has obvious advantages in terms of volume, cost, reliability and loss.	The single-phase half-bridge converter can only be used in low-power situations with low voltage level because of its high voltage stress and unbalanced capacitive voltage of bridge arm.
Single-phase Resonant Converters	[13]	Three-phase Inverter +Two LLC Resonant Tanks	1	42.5-50	1000	6/10	96.2%	It can realize bidirectional energy flow, simple structure, high power density, soft switching and wide voltage gain.	The excitation inductance is clamped by voltage, and the reverse voltage boost cannot be realized.
	[15]	Bidirectional CLLC Resonant Converter.	3.3	116	190-450	8/8	98%	It has the function of bidirectional pressure lifting and soft switching.	The structure is not symmetrical, which leads to the inconsistency of positive and negative operation characteristics, and increases the difficulty of parameter design.
	[16]	Bidirectional Full Bridge CLLC Resonant Converter	1	100	48-400	8/8	95%	It has the function of bidirectional operation and soft switching. The structure is symmetrical and the parameter design is simple.	The efficiency of the system needs to be improved.
Three-phase Resonant Converter	[17]	Paralleled CLLC Converters	2	100	200	16/16	96.6%	It has large system capacity, power density and better current sharing characteristics.	With the increase of charging power, large capacity filter capacitors occupy a lot of space.
	[14]	Three-Phase LLC Resonant Converter with A New Phase-shedding Technique	3	205	96	6/14	95	the three-phase structure provides higher power capacity and higher power density at higher power levels in comparison.	Limited gain range and poor light-load efficiency.
	[21]	+LLC+ Three-phase Full Bridge Rectifier	3	205	300-400	6/12	97.2%	It has soft switching characteristics and better power density and efficiency.	The peak current between the three phases is different, the temperature distribution is uneven, and the output current ripple is large.
Multiphase Interleaved Parallel Resonant Converter	[20]	Multiphase Interleaved DC/DC Converter	-	20	30	8/8	-		No soft switching technology is used, and the switching loss is high
	[18]	Two-phase Interleaved LLC Resonant Converter +Hybrid Rectifier	3.5	100	150-500	8/12	98%	It has soft switching characteristics and better power density and efficiency.	The current distribution between the two converters is not uniform, which is easy to damage the device.
	[19]	Two-phase Interleaved LLC Resonant Converter	1	60-150	400	8/16	92.08%	Multiphase interleaving can effectively reduce the output current ripple, and reduce the number of filter capacitors, so that each phase current is reduced, which is conducive to device selection.	The problem of uneven current between the two converters may exist in two-phase interleaving parallel, which will increase the current stress in the phase circuit and easily damage the device.
	[22]	IPOP+LLC Converter	1	100	400	8/16	94%		
	[23]	Interleaved LCLC Resonant Converter	1	170-250	12	10/6	96.7%		
	[24]	Three-Phase Y-Δ Interleaved Parallel CLLC Resonant Converter	1.5	200	48	12/12	93%		There is the problem of uneven flow in three-phase direct interleaving parallel, and there are more switching transistors, greater loss and complicated control.

II. ANALYSIS OF TOPOLOGY AND OPERATING CHARACTERISTICS OF BIDIRECTIONAL ON-BOARD CHARGING SYSTEM

A. STRUCTURE AND WORKING PRINCIPLE OF BIDIRECTIONAL ON-BOARD CHARGING SYSTEM

The topology of the bidirectional on-board charging system is shown in Fig. 3. The front-stage circuit is a bidirectional totem pole converter with a single-phase full-bridge structure, connected to the grid or AC electrical equipment. The rear-stage circuit is a three-phase wye-wye connected CLLC resonant converter connected to the power battery. The zero voltage turn-on characteristic of the resonant converter is used to reduce the switching loss of the converter, so as to improve the efficiency of the bidirectional on-board charging system. The on-board charging system can realize bidirectional flow of energy. The power battery can not only obtain power from the grid, but also invert its own power into single-phase alternating current output, which can be used as a temporary power source to provide power to external electrical equipment. According to the flow direction of electric energy, the bidirectional on-board charging system can be divided into forward charging operation mode and reverse inverting operation mode.

In charging mode, the front-stage converter is connected to the grid. On the one hand, it converts AC power to DC power to provide stable DC bus voltage for the rear-stage converter, and on the other hand, it realizes power factor correction to prevent harmonics from flowing into the grid. In the rear-stage converter, the primary-side switching transistors Q_1-Q_6 work in the high-frequency switching state, inverting the DC bus voltage into high-frequency voltage pulses. The secondary-side switching transistors Q_7-Q_{12} work in the rectification state to convert the high-frequency voltage pulses transmitted by the transformer into high-voltage DC output. In this operating mode, the output voltage on the DC side can be changed by changing the switching frequency of the switching transistors Q_1-Q_6 .

In the inverter mode, the secondary-side switching transistors Q_7-Q_{12} works in the high-frequency switching state in the rear-stage converter, inverting the DC power from the power battery into high-frequency voltage pulses, and the primary-side switching transistors Q_1-Q_6 works in the rectifier state, converting the high-frequency voltage pulses transmitted by the transformer into high-voltage DC output to the DC bus, providing stable high-voltage DC power for the front-stage converter. The front-stage converter works in the inverter mode, inverting the DC bus voltage to 220V AC output [25].

B. EQUIVALENT CIRCUIT MODEL OF RESONANT CONVERTER

Since the structure of the front-stage converter is relatively simple, this paper focuses on the rear-stage converter. In order to analyze the characteristics of the rear-stage converter, the equivalent circuit model is established by the fundamental

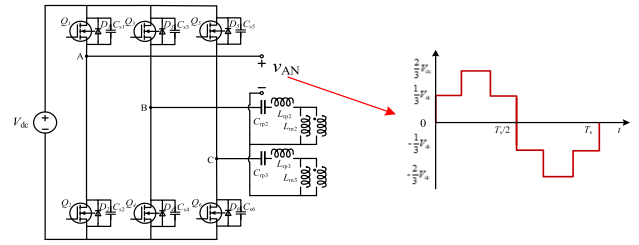


FIGURE 4. Inverter network and A-phase input voltage waveform.

wave analysis method, which only considers the fundamental components and ignores the influence of higher harmonics on the power conversion [26]. Reference [17] shows the equivalent circuit model established by fundamental wave analysis, and analyzes the voltage gain and impedance characteristics in detail. Taking phase A as an example, the equivalent model when it operates in forward charging mode is shown in Fig. 4.

The phase difference of the three-phase circuit of A, B and C is 120 degrees, and the input voltage v_{AN} of the resonant network is a step wave, neglecting the dead time, the expression of the input voltage v_{AN} in one resonant period T_s is:

$$v_{AN} = \begin{cases} \frac{V_{dc}}{3} & 0 \leq t < \frac{T_s}{6} \\ \frac{2V_{dc}}{3} & \frac{T_s}{6} \leq t < \frac{T_s}{3} \\ \frac{V_{dc}}{3} & \frac{T_s}{3} \leq t < \frac{T_s}{2} \\ -\frac{V_{dc}}{3} & \frac{T_s}{2} \leq t < \frac{2T_s}{3} \\ -\frac{2V_{dc}}{3} & \frac{2T_s}{3} \leq t < \frac{5T_s}{6} \\ -\frac{V_{dc}}{3} & \frac{5T_s}{6} \leq t < T_s \end{cases} \quad (1)$$

where T_s is the resonant period, $T_s = 1/f_s$, f_s is the switching frequency, V_{dc} is the DC voltage.

The fourier series v_{AN} can be expressed as:

$$v_{AN} = \frac{4V_{dc}}{3\pi} \left(\sin \omega_s t + \frac{1}{3} \sin 3\omega_s t + \dots + \frac{1}{n} \sin n\omega_s t \right) + \sum_{n=1}^{\infty} \left(\frac{V_{dc}}{3n\pi} (2 \cos n\pi - 2) \cdot \sin n\omega_s t \right) \quad (2)$$

where ω_s is the switching angular frequency, $\omega_s = 2\pi f_s$.

The fundamental component $v_{AN,FHA}$ and the rms value of the fundamental component $V_{AN,FHA}$ of v_{AN} are obtained from (2) as:

$$v_{AN,FHA} = \frac{4V_{dc}}{3\pi} \sin(\omega_s t) + \frac{2V_{dc}}{3n\pi} \sin(n\omega_s t) = \frac{2V_{dc}}{\pi} \sin(\omega_s t) \quad (3)$$

$$V_{AN,FHA} = \frac{\sqrt{2}}{\pi} V_{dc} \quad (4)$$

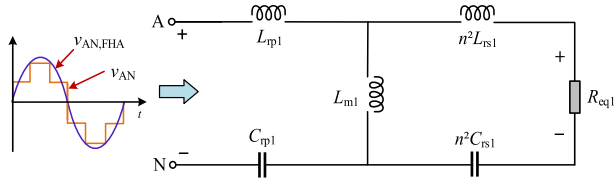


FIGURE 5. Equivalent circuit model of the rear-stage converter.

Similarly, the fundamental component $v_{DY,FHA}$ and the rms value of the fundamental component $V_{DY,FHA}$ of the resonant cavity voltage v_{DY} on the secondary-side are derived as:

$$v_{DY,FHA} = \frac{2V_{batt}}{\pi} \sin(\omega_s t + \phi) \quad (5)$$

$$V_{DY,FHA} = \frac{\sqrt{2}}{\pi} V_{batt} \quad (6)$$

where V_{batt} is the DC side input voltage.

The rear-stage equivalent circuit of the simplified converter obtained from the above derivation is shown in Fig. 5.

1) VOLTAGE GAIN ANALYSIS

According to the equivalent circuit model, the transfer function $G(s)$ of the converter can be found as in (7).

$$\begin{aligned} G(j\omega_s) &= \frac{nV_{batt}}{V_{dc}} = \frac{nV_{DY,FHA}}{V_{AN,FHA}} \\ &= \omega_s L_{m1} R_{eq} \left/ \left[R_{eq}(\omega_s L_{rp1} - \frac{1}{\omega_s C_{rp1}} + \omega_s L_{m1}) + j(\omega_s^2 L_{rp1}^2 \right. \right. \\ &\quad \left. \left. + 2\omega_s^2 L_{m1} L_{rp1} - \frac{2(L_{m1} + L_{rp1})}{C_{rp1}} + \frac{1}{\omega_s^2 C_{rp1}^2} \right) \right] \end{aligned} \quad (7)$$

where j is an imaginary unit, ω_s is the switching angular frequency, L_{m1} is the excitation inductance, L_{rp1} is the resonant inductance on the primary-side, C_{rp1} is the primary-side resonant capacitance.

According to the equivalent circuit model, the transfer function is normalized to obtain the expression for the DC voltage gain characteristic M :

$$\begin{aligned} M(f_n, Q, k) &= \frac{1}{\sqrt{\left(1 + \frac{1}{k} - \frac{1}{kf_n^2}\right)^2 + \frac{Q^2}{k^2} \left[(2k+1)f_n - \frac{2(k+1)}{f_n} + \frac{1}{f_n^3} \right]^2}} \end{aligned} \quad (8)$$

where f_n is the normalized frequency, k is the inductance factor, Q is the quality factor.

$$k = \frac{L_{m1}}{L_{rp1}} \quad (9)$$

$$f_n = \frac{f_s}{f_{r1}} = \frac{\omega_s}{2\pi f_{r1}} \quad (10)$$

$$Q = \frac{Z_o}{R_{eq}} \quad (11)$$

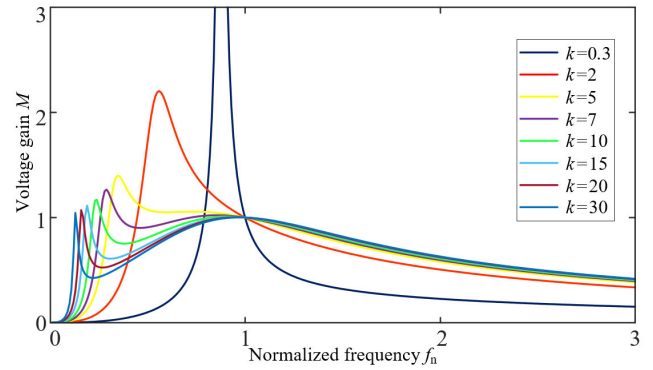


FIGURE 6. Voltage gain M at different k values for $Q = 0.4$.

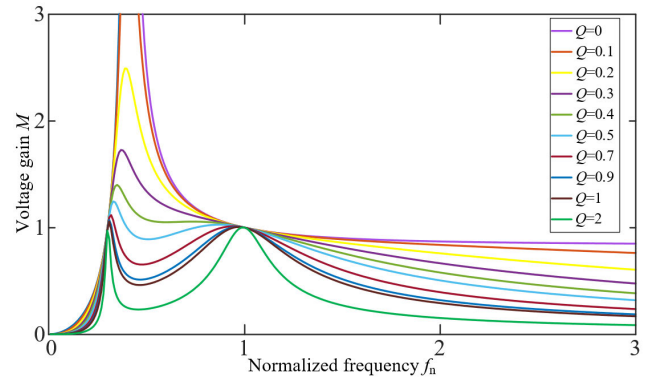


FIGURE 7. Voltage gain M at different Q values for $k = 5$.

where Z_o is the characteristic impedance, R_{eq} is the equivalent impedance.

$$Z_o = \sqrt{\frac{L_{rp1}}{C_{rp1}}} \quad (12)$$

As in (8), the voltage gain $M(f_n, Q, k)$ is related to f_n , Q , k . In order to analyze the effect of inductance coefficient k on $M(f_n, Q, k)$, Q is taken as a constant, and the relationship between $M(f_n, Q, k)$ and the variation of normalized frequency f_n and k is obtained with $Q = 0.4$, as shown in Fig. 6.

As can be seen from Fig. 6, when $f_n = 1$, the voltage gain $M(f_n, Q, k)$ is always 1, independent of the k value; as the k value increases, the voltage gain $M(f_n, Q, k)$ decreases at the same f_n . However, when the value of k decreases, the converter can obtain a wider voltage gain within the same normalized frequency.

Similarly, in order to analyze the effect of quality factor Q on $M(f_n, Q, k)$, the relationship between $M(f_n, Q, k)$ and the variation of normalized frequency f_n and Q is obtained with $k = 5$, as shown in Fig. 7.

As can be seen from Fig. 7, when $f_n = 1$, the voltage gain $M(f_n, Q, k)$ is always 1, independent of Q value; when Q value is small, the voltage gain $M(f_n, Q, k)$ decreases monotonically to the right of the maximum value, and a wider voltage gain can be obtained in a smaller f_n ; when Q value

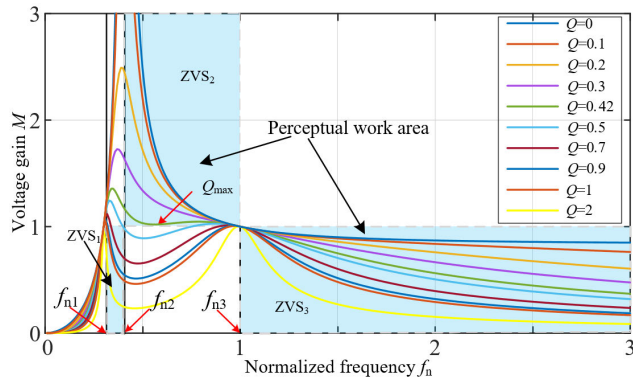


FIGURE 8. Inductive region of the rear-stage converter at $k = 5$.

increases, the voltage gain $M(f_n, Q, k)$ decreases in the same normalized frequency.

2) INPUT IMPEDANCE ANALYSIS

The prerequisite for a resonant converter to achieve zero voltage turn-on is that the input impedance exhibits inductance. According to the equivalent circuit of the rear-stage converter, the expression of the input impedance Z_{in} of the converter is obtained as:

$$Z_{in}(f_n, k, Q) = \sqrt{\frac{L_{rp1}}{C_{rp1}}} \left[\frac{Qk^2 f_n^6}{f_n^4 + Q^2(f_n - (k+1)f_n^3)^2} - j \frac{(f_n - (k+1)f_n^3)[Q^2((2k+1)f_n^2 - 1)(f_n^2 - 1) + f_n^2]}{f_n^4 + Q^2(f_n - (k+1)f_n^3)^2} \right] \quad (13)$$

Let the imaginary part of the input impedance of (13) be zero, and solve as:

$$\begin{cases} Q = \frac{f_n}{\sqrt{[(2k+1)f_n^2 - 1](1 - f_n^2)}} \\ f_{n2} = \frac{1}{\sqrt{k+1}} \end{cases} \quad (14)$$

where f_{n2} is the intrinsic resistive point.

It can be seen from Fig. 7 that if Q tends to infinity, there will be three points with positive and negative slope switching, and the other two resistive points can be solved as:

$$\begin{cases} f_{n1} = \frac{1}{\sqrt{2k+1}} \\ f_{n3} = 1 \end{cases} \quad (15)$$

For $k = 5$, the inductive region of the resonant converter is shown in Fig. 8.

From Fig. 8, when $f_n > 1$, the voltage gain curve always lies in the ZVS₃ inductive region, independent of Q . When $f_{n2} < f_n < 1$, the converter can cross from the ZVS₂ inductive region to the capacitive one as Q increases, so there is a critical value

TABLE 2. Design index of bidirectional on-board charging system.

Symbol	Parameters	Numerical value
V_{ac}	Positive AC side input voltage	176 V-264 V
V_{dc}	DC bus voltage	380 V-420 V
V_{batt}	Positive DC side output voltage	280 V-420 V
V_{batt}	Reverse DC side input voltage	300 V-400 V
V_{ac}	Reverse AC side output voltage	220 V
P_o	Rated power	3.3 kW
$\cos\phi$	Power factor	≥ 0.99
η	Overall machine efficiency	$\geq 94\%$

Q_{max} for Q . The maximum value of Q can be found by (14) as follows:

$$Q_{max} = \frac{1}{\sqrt{2k+1} - 1} \quad (16)$$

In order to ensure that the input impedance is inductive when $f_n > 1/(k+1)^{1/2}$, Q should be less than Q_{max} . In the ZVS₁ inductive region, the voltage gain of the converter is small. In the ZVS₂ and ZVS₃ regions, the voltage gain curve decreases monotonically as the normalized switching frequency increases, and the input impedance appears inductive, then the converter can achieve zero voltage turn-on in this region for the inverter-side switching transistors.

III. BIDIRECTIONAL ON-BOARD CHARGING SYSTEM PARAMETER DESIGN

A. DESIGN INDEX OF BIDIRECTIONAL ON-BOARD CHARGING SYSTEM

According to the actual demand, the design index of the bidirectional on-board charging system is shown in Table 2.

B. FRONT-STAGE CONVERTER PARAMETER DESIGN

1) INPUT INDUCTOR DESIGN

The front-stage converter stores and releases the energy of the input inductor L through the on and off of the main switching transistor. To ensure the stable operation of the front-stage converter, the input inductor should be designed for extremely input and output conditions.

Assuming the overall efficiency of the bidirectional on-board charging system is 94%, the input power of the bidirectional on-board charging system is:

$$P_{in} = \frac{P_o}{\eta} \approx 3.51kW \quad (17)$$

where P_o is the output power of the system, η is the efficiency of the system.

When the input voltage of the system fluctuates the most, that is, the input voltage is as low as 176 V, the current flowing through the inductor L is the maximum. The maximum effective value of the input current at this time is:

$$I_{in_max} = \frac{P_{in}}{V_{in_min}} \approx 19.94A \quad (18)$$

where V_{in_min} is the minimum input voltage.

The peak current of the input current is:

$$I_{in_peak} = \sqrt{2} \cdot I_{in_max} = 28.2A \quad (19)$$

Inductance current ripple is related to the size of the AC inductance, in engineering generally take the current ripple is 20% of the maximum current, the ripple current is:

$$\Delta I = 0.2 \cdot I_{in_peak} \approx 5.64A \quad (20)$$

The peak current flowing through the inductor L is:

$$I_{L_peak} = I_{in_peak} + \frac{\Delta I}{2} = 31.02A \quad (21)$$

At this point, the minimum duty cycle of the switching transistor is:

$$d = 1 - \frac{\sqrt{2}V_{in_min}}{V_{dc}} \approx 0.38 \quad (22)$$

where V_{dc} is the DC bus voltage.

$$L \geq \frac{\sqrt{2}V_{in_min} \cdot d}{f \cdot \Delta I} \approx 167.7\mu H \quad (23)$$

where f is the switching frequency of the switching transistors S_1 and S_2 ($f = 100$ kHz).

Since the ripple current is inversely proportional to the inductance value, a larger ripple current will increase the core loss. In order to ensure the normal operation of the front-stage converter, the final selected inductor parameter is $300 \mu H$.

2) DC BUS CAPACITOR DESIGN

The role of the DC bus capacitor is to provide a stable DC bus voltage for the rear-stage circuit, which needs to meet both the voltage maintenance time and ripple requirements. According to the conservation of energy, it is obtained that:

$$\frac{P_o}{\eta_{CLLC}} \cdot t_{hold} = \frac{C_{dc}V_{dc}^2}{2} - \frac{C_{dc}V_{dc_min}^2}{2} \quad (24)$$

where t_{hold} is the voltage maintenance time, η_{CLLC} is the efficiency of the rear-converter.

According to the actual demand, this paper takes the voltage maintenance time as one industrial frequency cycle of the input voltage, that is, $t_{hold} = 0.02$; the minimum DC bus voltage is taken as 80% of the rated value, that is, $V_{dc_min} = 320$ V; the efficiency of the rear-stage converter: $\eta_{CLLC} = 0.95$. According to (24), the capacitance value to meet the voltage maintenance time requirement is obtained as follows:

$$C_{dc1} = \frac{2P_o t_{hold}}{(V_{dc}^2 - V_{dc_min}^2) \cdot \eta_{CLLC}} \approx 2412\mu F \quad (25)$$

According to the conservation of energy it is known that:

$$V_{ac} \cdot I_L \cdot \eta_{PFC} = V_{dc} \cdot I_{out} \quad (26)$$

where V_{ac} is the AC voltage, η_{PFC} is the efficiency of the front-stage converter ($\eta_{PFC} = 0.98$).

$$i_{out} = \frac{V_{ac} \cdot I_L \cdot \eta_{PFC}}{V_{dc}} (1 - \cos(2\omega t)) \quad (27)$$

TABLE 3. Front-stage converter parameter design.

Symbol	Parameters	Numerical value
P_{in}	Input power	3.51 kW
I_{in_max}	Maximum effective value of the input current	19.94 A
I_{in_peak}	Peak current of the input current	28.2 A
ΔI	Ripple current	5.64 A
I_{L_peak}	Peak current flowing through the inductor L	31.02 A
d	Minimum duty cycle of the switching Transistor	0.38
L	Inductor	300 μH
C_{dc1}	Capacitance value to meet the voltage maintenance time requirement	2412 μF
C_{dc1}	Capacitance value to meet the voltage ripple requirement	1354 μF
C_{dc}	DC bus capacitor	2500 μF

where i_{out} is the output current.

The current flowing through the DC bus capacitor is:

$$i_{dc} = i_{out} - I_{out} = \frac{V_{ac} \cdot I_L \cdot \eta_{PFC}}{V_{dc}} \cos(2\omega t) \quad (28)$$

The amount of fluctuation of the DC bus voltage is:

$$\Delta v_{dc} = \frac{1}{C_{dc}} \int_0^t i_{dc}(t) dt = \frac{V_{ac} \cdot I_L \cdot \eta_{PFC}}{2\omega \cdot C_{dc} V_{dc}} \sin(2\omega t) \quad (29)$$

DC bus voltage ripple is:

$$\Delta V_{dc} = \frac{V_{ac} \cdot I_L \cdot \eta_{PFC}}{V_{dc} \cdot \omega \cdot C_{dc}} \quad (30)$$

In this paper, the maximum ripple of DC bus voltage is selected as ± 10 V, that is, $\Delta U_{dc} = 20$ V, and the capacitance value to meet the voltage ripple requirement can be obtained as follows:

$$C_{dc2} = \frac{V_{ac} \cdot I_L \cdot \eta_{PFC}}{V_{dc} \cdot \omega \cdot \Delta V_{dc}} = 1354\mu F \quad (31)$$

In summary, the maximum value of (25) and (31) is the lower limit of the DC bus capacitance of the front-stage converter, so the DC bus capacitor C_{dc} capacitance is chosen to be $2500 \mu F$.

The parameter design of the front-stage converter is shown in Table 3.

C. REAR-STAGE CONVERTER PARAMETER DESIGN

When the rear-stage converter works in forward mode, the input voltage range of the DC bus side is 380 V-420 V, and the output voltage range of the DC side of the power cell is 260 V-420 V; when it works in reverse mode, the input voltage range of the DC side of the power cell is 280 V-400 V, and the output voltage range of the DC bus side is 400 V; the rated power is 3.3 kW, and the first resonant frequency $f_{r1} = 100$ kHz. The relevant parameters are designed as follows:

1) TRANSFORMER TURNS RATIO

Taking the primary and secondary voltages at the first resonant frequency as the rated voltage of the converter and ignoring the diode voltage drop, the turns ratio n is:

$$n = \frac{V_{dc_nom}}{V_{batt_nom}} = \frac{400}{330} \approx 1.21 \quad (32)$$

2) VOLTAGE GAIN RANGE

The maximum voltage gain M_{max} and the minimum voltage gain M_{min} are:

$$M_{max} = \frac{n \times V_{batt_max}}{V_{dc_min}} = \frac{1.21 \times 420}{380} = 1.34 \quad (33)$$

$$M_{min} = \frac{n \times V_{batt_min}}{V_{dc_max}} = \frac{1.21 \times 280}{420} = 0.81 \quad (34)$$

3) DESIGN OF PARAMETERS K AND Q

At no load, the voltage gain of the converter is:

$$M_{NL}(k, f_n)|_{Q=0} = \frac{1}{1 + \frac{1}{k} - \frac{1}{kf_n^2}} \quad (35)$$

According to the maximum value of normalized switching frequency f_{n_max} and the minimum value of f_{n_min} in the design specification, the voltage gains at f_{n_max} and f_{n_min} at no load are obtained as follows:

$$\begin{cases} M_{NL_max}(f_{n_max})|_{Q=0} = \frac{(k+1)f_{n_max}^2 - 1}{kf_{n_max}^2} \\ M_{NL_min}(f_{n_min})|_{Q=0} = \frac{(k+1)f_{n_min}^2 - 1}{kf_{n_min}^2} \end{cases} \quad (36)$$

where $M_{NL_max}(f_{n_max})$ is the voltage gain at f_{n_max} , $M_{NL_min}(f_{n_min})$ is the voltage gain at f_{n_min} .

The minimum voltage gain M_{min} of the converter needs to be greater than $M_{NL_max}(f_{n_max})$, that is:

$$k < \frac{M_{min}(f_{n_max}^2 - 1)}{(1 - M_{min})f_{n_max}^2} \quad (37)$$

To prevent current overshoot during start-up, the start-up frequency is set at 300 kHz, which is known from (37):

$$k < \frac{M_{min}}{1 - M_{min}} \cdot \frac{(f_{n_max})^2 - 1}{(f_{n_max})^2} = 3.56 \quad (38)$$

According to the above analysis, as the value of k decreases, although the converter obtains a relatively wide voltage gain within the same operating frequency, the excitation inductance L_{m1} is proportional to k , resulting in an increase in the excitation current i_{Lm1} , then the loss of the switching transistor increases during the dead time. Taking into account, temporarily take $k = 3.5$. This results in:

$$Q_{max} = \frac{1}{\sqrt{2k+1}-1} \approx 0.55 \quad (39)$$

where the prime factor Q_{max} is the resistive boundary line of the converter.

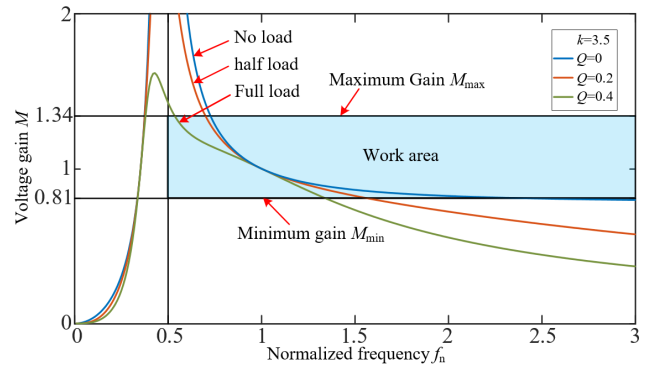


FIGURE 9. Voltage gain at full load, half load and no load.

$Q = 0.4$ in order to retain a certain margin.

From Fig. 9, it can be seen that the converter can meet the voltage gain requirements in the designed operating frequency range under full-load, half-load and no-load conditions. Therefore, the parameters k and Q are taken as reasonable values.

4) RESONANT CAVITY PARAMETERS

The values of the resonant inductor and resonant capacitor are calculated according to the values of the parameters k and Q , and the first resonant frequency f_{r1} . The equivalent impedance of the converter is given by:

$$R_{eq} = n^2 \frac{6}{\pi^2} \frac{V_{batt_nom}^2}{P_o} \approx 29.4\Omega \quad (40)$$

Resonant inductor on the primary-side:

$$L_{rp1} = \frac{QR_{eq}}{2\pi f_{r1}} = 18.73\mu H \quad (41)$$

Resonant inductor on the secondary-side:

$$L_{rs1} = \frac{L_{rp1}}{n^2} = 12.79\mu H \quad (42)$$

Resonant capacitance on the primary-side:

$$C_{rp1} = \frac{1}{(2\pi f_{r1})^2 \cdot L_{rp1}} = 135.38nF \quad (43)$$

Resonant capacitance on the secondary-side:

$$C_{rs1} = n^2 C_{rp1} = 198.21nF \quad (44)$$

Excitation inductance:

$$L_{m1} = kL_{rp1} = 65.54\mu H \quad (45)$$

5) SWITCHING FREQUENCY

In order to design the transformer, it is necessary to determine the operating frequency at which the converter meets the maximum gain. The operating frequency is generally selected by fundamental wave analysis (FHA), simulation or time domain analysis. The fundamental wave analysis method is more accurate at the resonance point, but it cannot give a

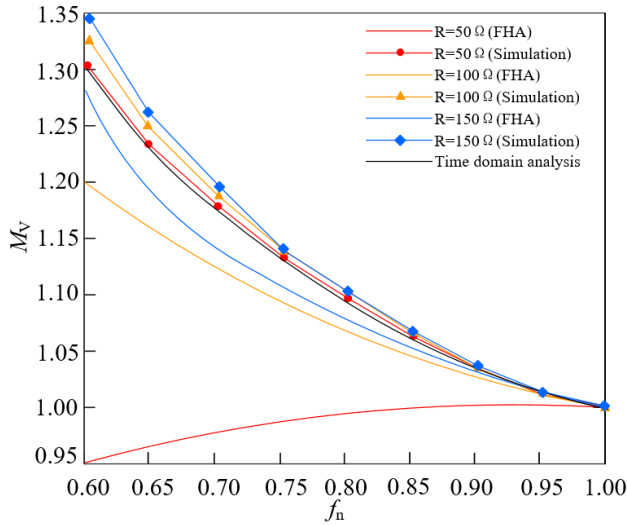


FIGURE 10. Comparison of gain obtained by fundamental wave analysis, time domain analysis and simulation (under resonant state).

more accurate voltage gain when it is far from the resonance point, so the specific operating frequency range cannot be determined.

a: Under resonant operating mode

When the system is in under resonant operation mode, the CLLC resonant converter can realize zero voltage on the inverter side of the switching transistor and zero current off the rectifier side of the diode, which is an ideal operation mode. The design of parameters should ensure that the CLLC resonant converter can run stably in this mode. Fig. 10 shows the comparison of gains obtained by time domain analysis, fundamental wave analysis and simulation. It can be seen that the time domain analysis method can better approximate the actual gain curve.

b: Over resonant operation mode

When the system is in over resonant working mode, the comparison of the gain curves in the over-resonant region obtained by simulation, time domain analysis and fundamental wave analysis is shown in Fig. 11. It can be seen that whether it is full load or no load, the time domain analysis method can approach the actual gain curve well, and compared with the fundamental wave analysis method, the accuracy has been greatly improved.

Comparing the data obtained from the time domain analysis method, simulation and experiment, it is concluded that the results of the time domain analysis method and simulation match, and the accuracy is greatly improved compared with the fundamental wave analysis method. Therefore, the operating frequency range of the converter is 65 kHz-300 kHz obtained by simulation.

Due to the large number of resonant components in the three-phase wye-wye connected CLLC resonant converter, if the parameters of the three-phase resonant network are the

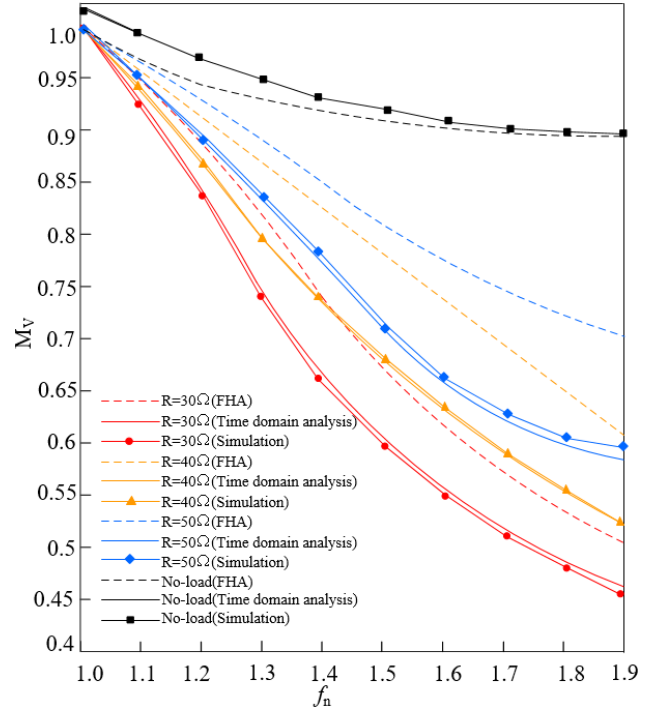


FIGURE 11. Comparison of gain obtained by fundamental wave analysis, time domain analysis and simulation (over resonant state).

same and the primary-side is symmetrical in parameters, the number of variables in the system is reduced, and the DC voltage gain is the same in the same operating frequency range during forward and reverse operation. The difference of the working state of the three-phase circuit A, B and C is only shown as A phase difference of 120 degrees, and the other states are exactly the same. Therefore, the basic characteristics and parameter design of the three-phase interleaved CLLC resonant converter can be regarded as a single-phase CLLC resonant converter. This paper takes the A-phase circuit as an example for analysis. According to the different state of the resonant network, the converter has two different resonant frequencies: one is that the resonant network is composed of L_{rp1} , L_{rs1} , C_{rp1} , C_{rs1} four components, and the first resonant frequency is f_{r1} ; The other is that the resonant network is composed of L_{rp1} , C_{rp1} , L_{m1} , C_{rs1} , L_{rs1} five components, and this is the second resonant frequency f_{r2} . The expressions for f_{r1} and f_{r2} are:

$$f_{r1} = \frac{1}{2\pi\sqrt{L_{rp1}C_{rp1}}} \tag{46}$$

$$f_{r2} = \frac{1}{2\pi\sqrt{(L_{rp1} + L_{m1})C_{rp1}}} \tag{47}$$

With the first resonant frequency f_{r1} and the second resonant frequency f_{r2} as the boundary, according to the different switching frequency f_s , the three operating conditions of the three-phase interleaved CLLC resonant converter are as follows: the under resonant operating mode meets $f_{r2} < f_s < f_{r1}$; The working mode of resonant point satisfies

TABLE 4. Rear-stage converter parameter design.

Symbol	Parameters	Numerical value
n	Transformer ratio	1.21
M_{max}	Maximum voltage gain	1.34
M_{min}	Minimum voltage gain	0.81
Q_{max}	Resistive boundary line	0.55
R_{eq}	Equivalent impedance	29.4 Ω
L_{rp1}	Primary-side resonant inductor	18.73 μH
C_{rp1}	Primary-side resonant capacitance	135.38 nF
L_{rs1}	Secondary-side resonant inductor	12.79 μF
C_{rs1}	Secondary-side resonant capacitance	198.21 nF
L_m	Excitation inductance	65.54 μH

$f_s = f_{r1}$; The over resonant operating mode is $f_s > f_{r1}$. The higher the switching frequency, the smaller the current ripple value and the higher the power quality. In addition, the volume of capacitors, inductors, transformers and other devices is also affected by the switching frequency, the higher the switching frequency, the smaller the volume of these devices, which can improve the power density of the whole machine. However, if the switching frequency is too high, it will cause the increase of other losses such as switching loss and driving loss, resulting in a decrease in system efficiency. Considering the performance index comprehensively, the switching frequency of the system is set as the first resonant frequency of 100kHz, and the performance of the system is optimal.

The parameter design of the rear-converter is shown in Table 4.

IV. BIDIRECTIONAL ON-BOARD CHARGING SYSTEM CONTROL STRATEGY

A. FRONT-STAGE CONVERTER CONTROL STRATEGY

The front-stage converter control strategy is shown in Fig. 12. In the forward charging mode, the front-stage converter realizes the rectification and power factor correction function, and in the reverse inverting mode, the front-stage converter realizes the inverting function. Since in the forward charging and reverse inverting operation modes, only the controlled objects are different, so this paper only analyzes the control strategy specifically for the forward charging operation mode. The reference voltage v_{dc_ref} and the DC bus voltage v_{dc} are differenced, and the error is multiplied by the voltage PI regulator and the input voltage to get the current loop control quantity, and then differenced from the input current i_L to get the current error quantity, and then the switching frequency required by the switching transistor is generated by the current PI regulator and pulse frequency modulation to realize the constant voltage output.

B. REAR-STAGE CONVERTER CONTROL STRATEGY

The control strategy of the rear-stage converter is shown in Fig. 13. In the forward charging operation mode, in order to realize the constant voltage and constant current charging

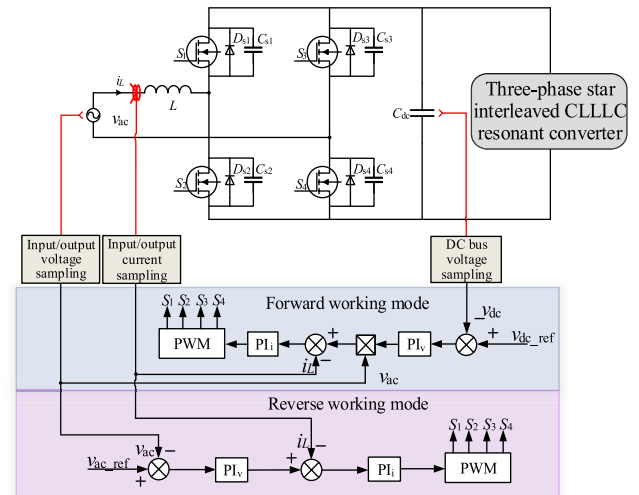


FIGURE 12. Front-stage converter control strategy.

mode of the power battery, the voltage and current double closed-loop control is used. When the rear-stage converter works in constant voltage output mode, the control object is the output voltage V_{batt} , and the difference with the given reference voltage V_{batt_ref} is made to get the error quantity V_{err} , and the error quantity V_{err} gets the voltage loop control quantity V_n through the voltage PI regulator and limiting link, and V_n generates the switching frequency required by Q_1-Q_6 through pulse frequency modulation to realize constant voltage output. When the rear-stage converter works in constant current output mode, the control object is the output current I_{batt} , and the difference with the given reference current I_{batt_ref} is made to get the error quantity I_{err} , and I_{err} gets the current loop control quantity I_n through the current PI regulator and limiting link, and I_n generates the required pulses of Q_1-Q_6 through pulse frequency modulation to realize the constant current output of the converter. In the reverse inverter operation mode, the reference voltage of the control system is V_{dc_ref} , and the DC bus voltage is stabilized at 400V by adjusting the switching frequency of Q_7-Q_{12} .

V. EXPERIMENTAL ANALYSIS OF BIDIRECTIONAL ON-BOARD CHARGING SYSTEM

The experimental platform of the bidirectional on-board charging system based on the rear-stage three-phase wye-wye connected CLLC resonant converter is shown in Fig. 14, and its hardware structure is shown in Fig. 15.

A. THE MAIN COMPONENTS SELECTION

1) SELECTION OF SWITCHING TRANSISTORS

IPW65R045C7 switching transistor was selected for both the primary and secondary sides. The drain-source voltage $V_{dss} = 650 \text{ V}$, the on-impedance $R_{ds(on)_max} = 0.045 \Omega$, the parasitic capacitance $C_{oss} = 70 \text{ pF}$, and the maximum continuous leakage current was $I_D = 68.5 \text{ A}$. Dead time $t_{dead} = 200 \text{ ns}$.

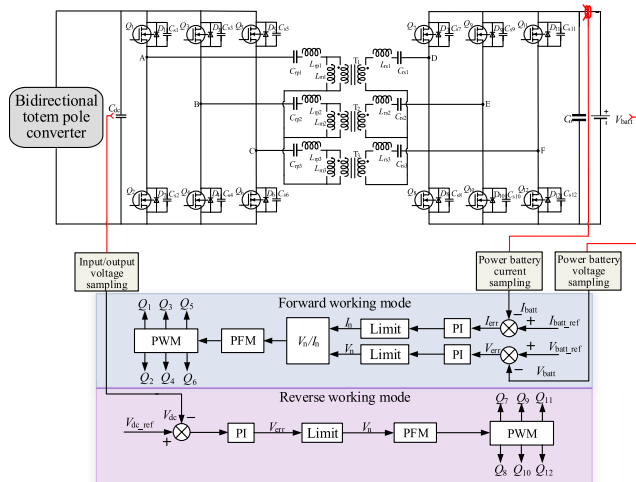


FIGURE 13. Rear-stage converter control strategy.

2) TRANSFORMER DESIGN

The magnetic core model is determined to be EE50, and its parameters are: $AP = 5.7343 \text{ cm}^4$, $A_e = 226 \text{ mm}^2$, $A_w = 253 \text{ mm}^2$. The number of primary and secondary side turns is 22 and 18 respectively. Select the Leeds wire with $d = 0.1 \text{ mm}$, and the number of Leeds wire strands required for each turn of the primary and secondary conductors is 217 and 240 strands, respectively. Magnetic flux density $B_m = 0.29 \text{ T}$, window coefficient $D_w = 0.28$.

3) SELECTION OF RESONANT INDUCTORS

The primary-side resonant inductor is selected as 8 turns 217 strands, the secondary-side resonant inductor as 6 turns 240 strands, and the number of strands of each turn wire is 217 and 240 strands respectively.

4) SELECTION OF PWM OF RESONANT CAPACITANCE

The primary-side resonant capacitors L_{rp1} , L_{rp2} , and L_{rp3} are composed of four 33 nF/1000 V polypropylene capacitors and one 3.3 nF/1000 V polypropylene capacitor in parallel. Similarly, the secondary side resonant capacitors C_{rs1} , C_{rs2} , and C_{rs3} are composed of five 39 nF/1000 V, one 2.2 nF/1000 V, and one 1 nF/1000 V polypropylene capacitors in parallel.

B. CHARGING MODE

When the bidirectional on-board charging system is in charging mode, the input voltage and input current of the system are shown in Fig. 16. As can be seen from Fig. 16, the input current follows the input voltage in frequency and phase, the input voltage is 220 V, the peak current is about 20 A, and the system has a high power factor.

When the rear-stage converter operates at 100 kHz, the driving waveforms of the three lower transistors of the bridge arms on the primary-side are shown in Fig. 17. The three resonant networks are interleaved 120 degrees by controlling the drive signal. The phase difference between the driving

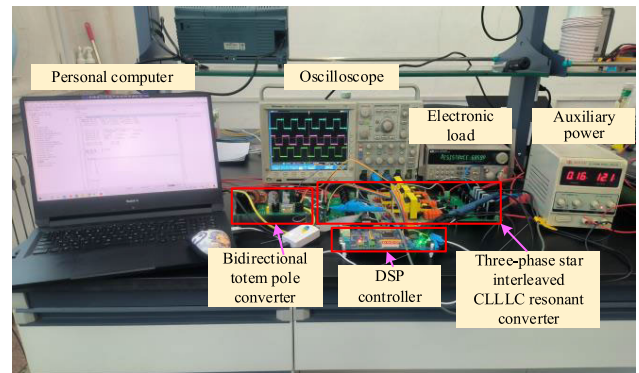


FIGURE 14. Experimental platform of bidirectional on-board charging system.

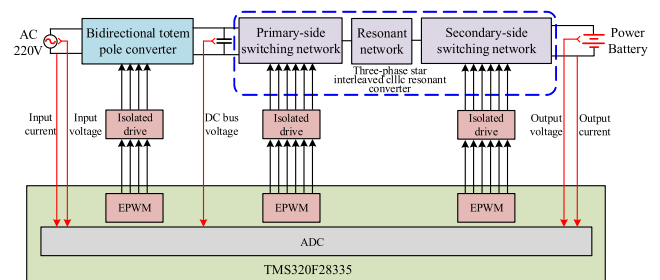


FIGURE 15. Hardware block diagram of bidirectional on-board charging system.

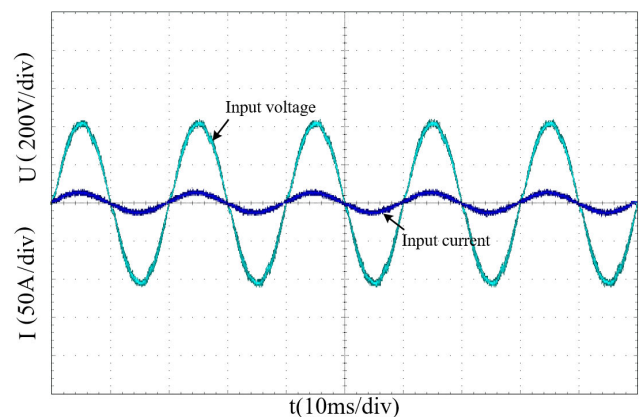


FIGURE 16. Input voltage and input current waveforms.

voltages of switching transistors Q_1 , Q_3 and Q_5 are all 120 degrees.

The driving signals of the bridge arm switch transistors Q_1 and Q_2 on the primary-side of the rear-stage converter and the input voltage waveform of the A-phase circuit are shown in Fig. 18. In order to prevent simultaneous conduction of the upper and lower transistors of the same bridge arm, a certain dead time needs to be preserved, and the input voltage waveform of the resonant network of the A-phase circuit is a step waveform, which is consistent with the theoretical analysis and simulation results.

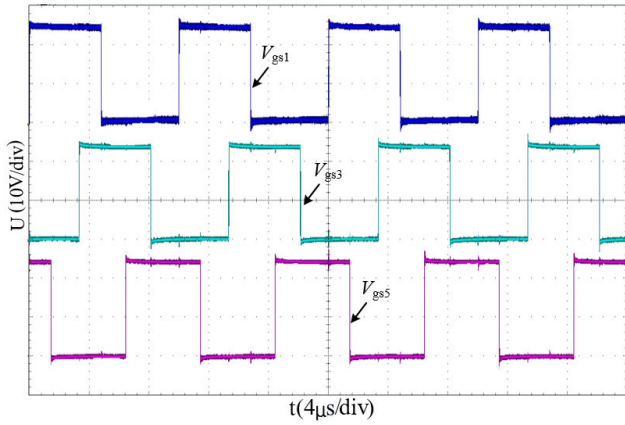


FIGURE 17. Driving voltage waveforms of switching transistors Q_1 , Q_3 and Q_5 .

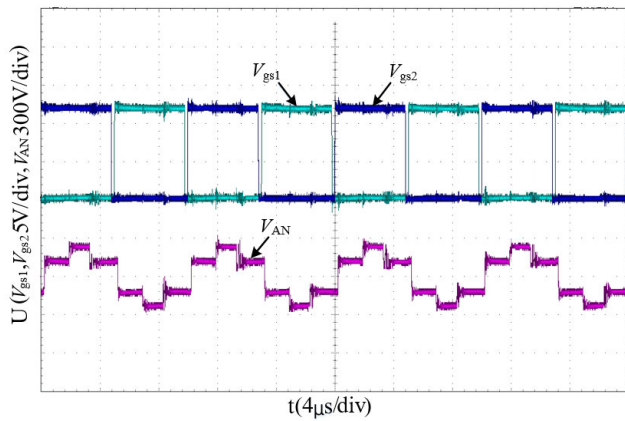


FIGURE 18. Driving of switching transistors Q_1 and Q_2 and input voltage waveform of phase A circuit.

The input voltage waveforms of the three-phase circuit of the rear-stage converter A, B and C are shown in Fig. 19. As can be seen from the Fig. 19, the input voltage waveforms of A, B and C three-phase circuits differ in phase by 120 degrees, and they are all step waveforms, with the maximum magnitude being two-thirds of the DC bus voltage, and when the DC bus voltage is 400 V, the maximum magnitude of the input step voltage is about 266 V.

When the rear-stage converter operates at the rated resonant frequency of 100 kHz, the waveforms of the drive signal, drain-source voltage and resonant current of the switching transistor Q_1 are shown in Fig. 20. At this operating frequency, the resonant inductor and capacitor on the primary-side resonate in series, and the resonant current is approximately sinusoidal. The resonant current crosses the zero point after the drive signal goes high, so the input impedance of the converter is inductive.

The waveforms of the drive signal V_{gs1} and the gate-source voltage V_{ds1} are shown in Fig. 21. It can be seen that the switching transistor Q_1 achieves zero voltage turn-on.

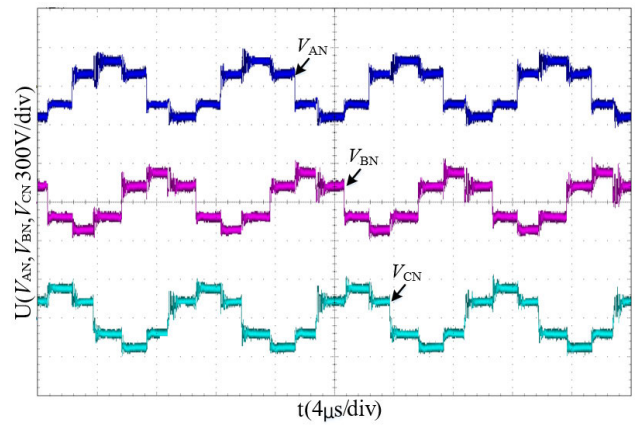


FIGURE 19. A, B, C three-phase circuit input voltage waveforms.

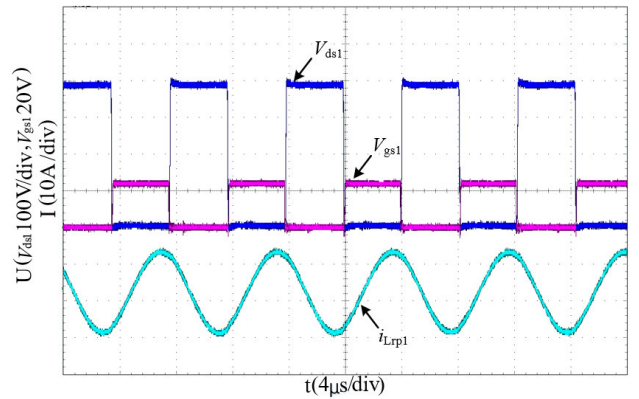


FIGURE 20. Waveforms of drive signal, drain-source voltage and resonant current of switching transistor Q_1 at 100kHz.

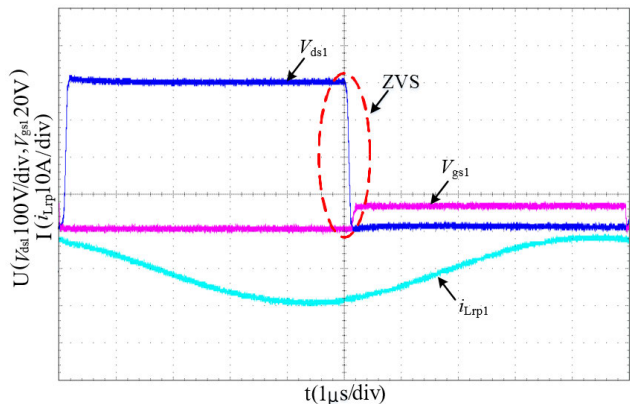


FIGURE 21. Waveforms of drive signal V_{gs1} and gate-source voltage V_{ds1} .

When the rear-stage converter operates at the rated resonant frequency of 100 kHz, the waveforms of the DC side output voltage and the three-phase resonant current on the primary-side are shown in Fig. 22. As can be seen from the Fig. 22, the three-phase resonant currents are symmetrical, indicating that the three-phase wye-wye connected topology has good current equalization characteristics.

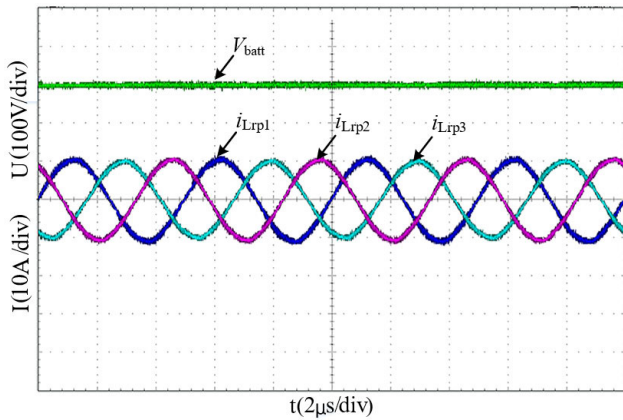


FIGURE 22. Waveforms of output voltage and three-phase resonant current on the primary-side.

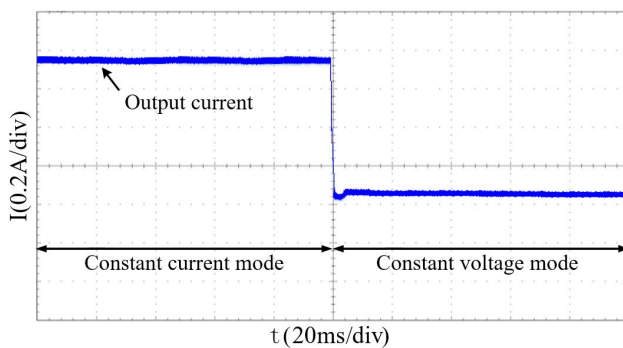


FIGURE 23. Output current waveform.

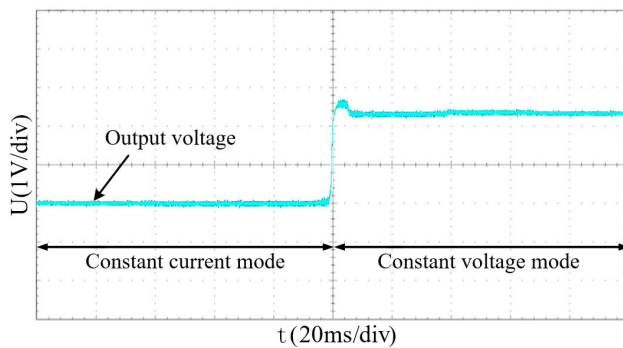


FIGURE 24. Output voltage waveform.

In order to verify the charging performance of constant current and constant voltage charging system. The charging current of constant current charging mode is set to 10 A, and the charging voltage of constant voltage charging mode is set to 400 V. As shown in Fig. 23, when the constant current charging mode is used, the output current remains basically unchanged when it is stabilized at 10 A, thus realizing the control of constant current charging. Then, the output current is switched from constant current mode to constant voltage mode, and the output current is in a stable state after a step drop. As shown in Fig. 24, when the constant current charging

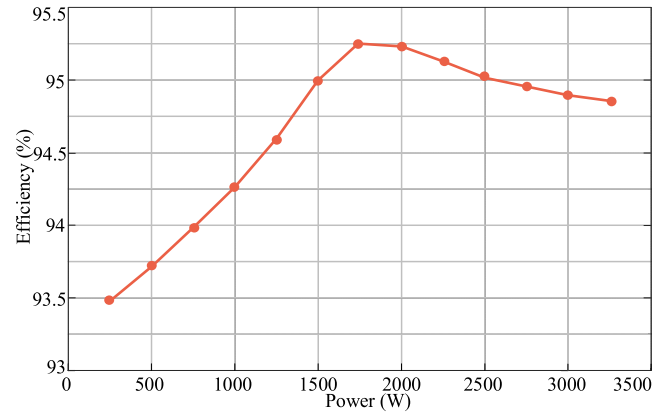


FIGURE 25. The efficiency curve of the system in charging mode.

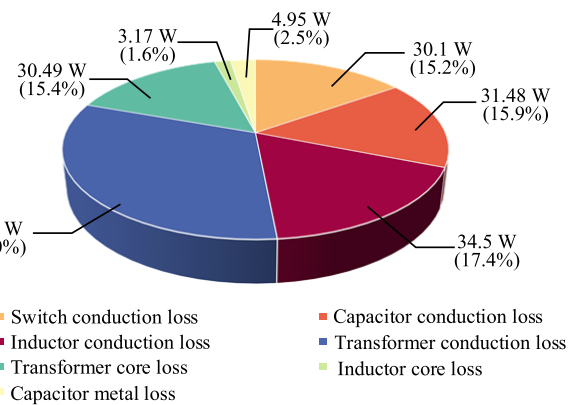


FIGURE 26. The efficiency curve of the system in charging mode.

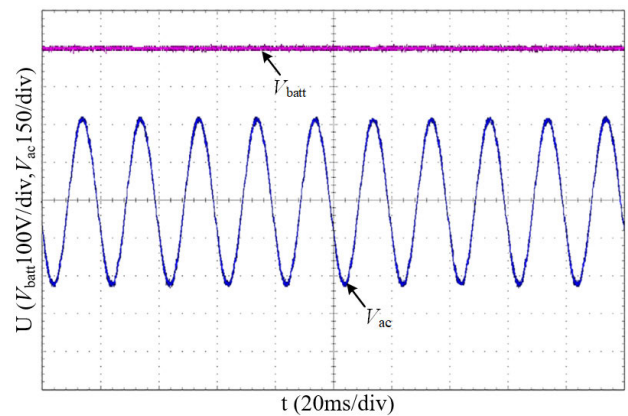


FIGURE 27. Inverter output voltage waveform.

mode is used, the output voltage is in a stable state, and then it is switched from the constant current mode to the constant voltage mode, and the output voltage remains basically unchanged after stabilizing at 440 V. Thus, the system can control constant current charging and constant voltage charging.

Fig. 25 shows the efficiency curve of the system when the rated power changes in the charging mode. As can

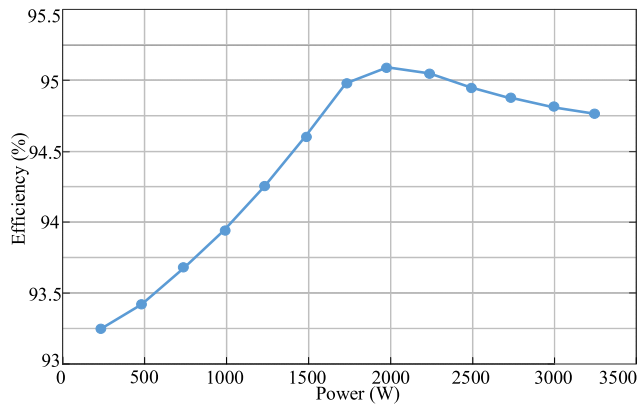


FIGURE 28. The efficiency curve of the system in inverter mode.

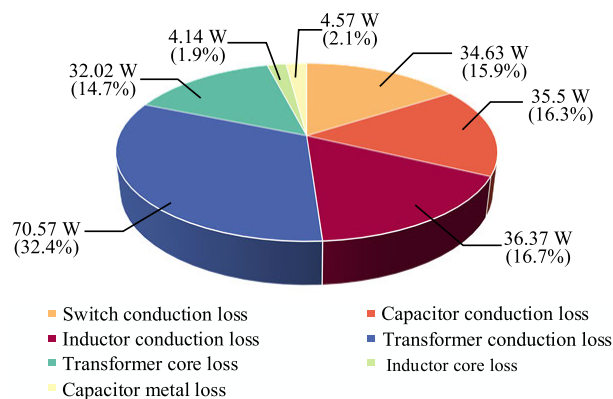


FIGURE 29. Loss decomposition of the system in inverter mode.

be seen from the figure, the system has a high working efficiency, the highest efficiency can reach more than 95%.

Fig. 26 shows the loss distribution of the system when the system works in the charging mode and the highest working efficiency point. The total loss is 198W.

C. INVERTER MODE

In inverter mode, the inverter output waveform of the front-stage converter is shown in Fig. 27. It can be seen that the input voltage of DC side is 400 V, and the inverter output is 311 V AC power, frequency is 50 Hz, which can supply power to external devices, verifying that the bidirectional on-board charging system can realize the bidirectional flow of energy.

Fig. 28 shows the efficiency curve of the system when the rated power changes in the inverter mode. As can be seen from the figure, the system has a high working efficiency, the highest efficiency can reach more than 95%.

Fig. 29 shows the loss distribution of the system when the system works in inverter mode and at the highest working efficiency point. The total loss is 271.8W.

VI. CONCLUSION

This paper proposes a bidirectional on-board charging system with a two-stage isolated structure. The front-stage converter can realize the bidirectional flow of energy, the forward operating mode realizes the function of rectification and power factor correction, while the reverse operating mode inverts the output AC power. The relationship between the voltage, current and control signal of the front-stage converter is deduced through the small signal analysis method. In addition, the equivalent circuit model of the rear-stage converter is established by the fundamental wave analysis method, and the voltage gain characteristics and impedance characteristics are then analyzed. Through simulation and experimental verification, the bidirectional on-board charging system based on three-phase wye-wye connected CLLC resonant converter can realize bidirectional energy flow, the front-stage converter has high power factor, and the rear-stage converter can realize zero voltage turn-on in the full load range.

REFERENCES

- [1] M. R. Khalid, I. A. Khan, S. Hameed, M. S. J. Asghar, and J.-S. Ro, "A comprehensive review on structural topologies, power levels, energy storage systems, and standards for electric vehicle charging stations and their impacts on grid," *IEEE Access*, vol. 9, pp. 128069–128094, 2021.
- [2] L. Qu, X. Wang, J. Xu, and H. Liu, "Design method of bidirectional CLLC resonant converter for on-board charger applications," *J. Harbin Inst. Technol.*, vol. 53, no. 9, pp. 144–155, Sep. 2021.
- [3] J. Yuan, L. Dorn-Gomba, A. D. Callegaro, J. Reimers, and A. Emadi, "A review of bidirectional on-board chargers for electric vehicles," *IEEE Access*, vol. 9, pp. 51501–51518, 2021.
- [4] F. E. U. Reis, R. P. Torrico-Bascopé, F. L. Tofoli, and L. D. Santos Bezerra, "Bidirectional three-level stacked neutral-point-clamped converter for electric vehicle charging stations," *IEEE Access*, vol. 8, pp. 37565–37577, 2020.
- [5] Y. Mei, W. Huang, and Z. Liu, "Bidirectional and isolated AC–DC converter based on reduced matrix converter," *Trans. China Electrotech. Soc.*, vol. 34, no. 12, pp. 2499–2506, Jun. 2019.
- [6] Y. Xu, Z. Wang, Y. Shen, Z. Zou, and M. Liserre, "A VSC based isolated matrix-type AC/DC converter without bidirectional power switches," *IEEE Trans. Ind. Electron.*, vol. 70, no. 12, pp. 1–11, Dec. 2023.
- [7] S. Chen, W. Yu, and D. Wang, "Bidirectional H8 AC–DC topology combining advantages of both diode-clamped and flying-capacitor three-level converters," *IEEE J. Emerg. Sel. Topics Power Electron.*, vol. 10, no. 4, pp. 3643–3651, Aug. 2022.
- [8] L. Zhu, Z. Sheng, F. Peng, and L. Yang, "Control strategy of half-bridge three-level LLC resonant converters with wide output voltage range," *IEEE Trans. Plasma Sci.*, vol. 50, no. 11, pp. 4381–4386, Nov. 2022.
- [9] H. Huang, Z. Chen, and H. Wang, "Zero sequence voltage injection to control neutral potential balance of three-level NPC," *J. Electron. Meas. Instrum.*, vol. 34, no. 6, pp. 138–143, Jun. 2020.
- [10] X. Chen, M. Wang, C. Li, N. Zhao, and Z. Zheng, "Optimum total losses orientated modulation strategy for dual active bridge," *J. Electr. Eng.*, vol. 17, no. 2, pp. 49–55, Jun. 2022.
- [11] A. K. Singh, A. K. Mishra, K. K. Gupta, and Y. P. Siwakoti, "High voltage gain bidirectional DC–DC converters for supercapacitor assisted electric vehicles: A review," *CPSS Trans. Power Electron. Appl.*, vol. 7, no. 4, pp. 386–398, Dec. 2022.
- [12] X. Li, J. Huang, Y. Ma, X. Wang, J. Yang, and X. Wu, "Unified modeling, analysis, and design of isolated bidirectional CLLC resonant DC–DC converters," *IEEE J. Emerg. Sel. Topics Power Electron.*, vol. 10, no. 2, pp. 2305–2318, Apr. 2022.

- [13] M. Salem, V. K. Ramachandaramurthy, A. Jusoh, S. Padmanaban, M. Kamarol, J. Teh, and D. Ishak, "Three-phase series resonant DC-DC boost converter with double LLC resonant tanks and variable frequency control," *IEEE Access*, vol. 8, pp. 22386–22399, 2020.
- [14] S. A. Arshadi, M. Ordonez, W. Eberle, M. Craciun, and C. Botting, "Three-phase LLC battery charger: Wide regulation and improved light-load operation," *IEEE Trans. Power Electron.*, vol. 36, no. 2, pp. 1519–1531, Feb. 2021.
- [15] F. Wang, F. Zhang, H. Dai, and Z. Wang, "Optimized design of CLLC bi-directional resonant converter based on time domain analysis," *Power Electron.*, vol. 53, no. 6, pp. 80–82, Jun. 2019.
- [16] Q. Chen, Y. Ji, and J. Wang, "Analysis and design of bidirectional CLLC resonant DC-DC transformers," *Proc. Chin. Soc. Electr. Eng.*, vol. 34, no. 18, pp. 2898–2905, Jun. 2014.
- [17] X. Wang, B. Liu, L. Jiang, and Z. Zhan, "Current sharing analysis for novel paralleled CLLC converters," *IEEE Access*, vol. 9, pp. 141307–141320, 2021.
- [18] H. Wu, X. Zhan, and Y. Xing, "Interleaved LLC resonant converter with hybrid rectifier and variable-frequency plus phase-shift control for wide output voltage range applications," *IEEE Trans. Power Electron.*, vol. 32, no. 6, pp. 4246–4257, Jun. 2017.
- [19] Y. Yang, H. Wu, and T. Guan, "Magnetic integrated current sharing characteristics of interleaved LLC resonant converter," *Trans. China Electrotech. Soc.*, vol. 34, no. 12, pp. 2529–2538, Jun. 2019.
- [20] B. Su, Y. Wang, F. Wang, Z. Guo, and Y. Dong, "Multi-phase interleaved bidirectional DC-DC converter with coupled inductors and current sharing control strategy," *Trans. China Electrotech. Soc.*, vol. 35, no. 20, pp. 4336–4349, Oct. 2020.
- [21] S. A. Arshadi, M. Ordonez, W. Eberle, M. A. Saket, M. Craciun, and C. Botting, "Unbalanced three-phase LLC resonant converters: Analysis and trigonometric current balancing," *IEEE Trans. Power Electron.*, vol. 34, no. 3, pp. 2025–2038, Mar. 2019.
- [22] Y. Yang, S. Deng, and J. Yao, "Research on current sharing characteristics of interleaved LLC resonant converter based on fully coupled inductor," *Electr. Mach. Control*, vol. 24, no. 12, pp. 86–96, Dec. 2020.
- [23] M. Forouzes and Y.-F. Liu, "Interleaved LCLC resonant converter with precise current balancing over a wide input voltage range," *IEEE Trans. Power Electron.*, vol. 36, no. 9, pp. 10330–10342, Sep. 2021.
- [24] Y. Yang, B. Hou, and H. Li, "Three-phase interleaved bidirectional CLLC resonant converter," *Electr. Mach. Control*, vol. 25, no. 9, pp. 121–131, Sep. 2021.
- [25] K. Zhou, S. Zheng, N. Jin, and D. Sun, "Two-stage isolated bidirectional on-board charger and control technology," *J. Electr. Hybrid Veh.*, vol. 13, nos. 3–4, pp. 362–386, Mar. 2021.
- [26] Q. Deng, Y. He, C. Lei, and J. Liu, "CLLC resonant converter variable frequency phase shift hybrid control method," *Electr. Power Autom. Equip.*, vol. 42, no. 2, pp. 148–154, Feb. 2022.



KAI ZHOU received the B.S. degree in communication engineering from Qiqihar University, Qiqihar, China, in 2006, and the M.S. and Ph.D. degrees in electrical engineering from the Harbin University of Science and Technology (HUST), Harbin, China, in 2009 and 2012, respectively.

He is currently a Professor with HUST and the Deputy Director of the Engineering Research Center of Automotive Electronics Drive Control and System Integration, Ministry of Education.

His research interests include power electronics system of new energy vehicles, automotive electronics control technology, and automotive electronics testing technique.



YIWEN HUANG received the B.S. degree in electrical engineering from the Harbin University of Science and Technology (HUST), Harbin, China, in 2018, where she is currently pursuing the M.S. degree.

She has participated in the Heilongjiang Provincial Natural Science Foundation of China and mainly completed the charging direction of integrated on-board charging systems. Her research interests include on-board charging and electric energy conversion.



SHAOLONG ZHENG received the B.S. degree in electrical engineering from the Anhui University of Technology, Anhui, China, in 2020, and the M.S. degree in electrical engineering from the Harbin University of Science and Technology (HUST), Harbin, China, in 2023.

He has participated in the Heilongjiang Provincial Natural Science Foundation of China and mainly completed the driving direction of integrated on-board charging systems. His current research interests include on-board charging and power conversion.

...